Influence of Hydroxycoumarin Substituents on the Photophysical Properties of Chiroptical Tb(III) and Eu(III) Complexes

Influence of Hydroxy-Coumarin Substituents on the Photophysical properties of Chiroptical Tb(III) and Eu(III) Complexes

Silvia Ruggieri, Silvia Mizzoni, Enrico Cavalli, Cristina Sissa, Michele Anselmi, Andrea Gualandi, Pier Giorgio Cozzi, Albano N. Carneiro Neto, Andrea Melchior, Francesco Zinna, Oliver G. Willis, Lorenzo Di Bari, Fabio Piccinelli

DOI: 10.1021/acs.inorgchem.4c03541

Influence of Hydroxy-Coumarin Substituents on the Photophysical properties of Chiroptical Tb(III) and Eu(III) Complexes

Silvia Ruggieri,[1] Silvia Mizzoni,[1] Enrico Cavalli,[2] Cristina Sissa,[2] Michele Anselmi,[3] Andrea Gualandi,[3,4] Pier Giorgio Cozzi,[3,4] Albano N. Carneiro Neto,[5] Andrea Melchior,[6*] Francesco Zinna,[7] Oliver G. Willis,[7] Lorenzo Di Bari,[7*] Fabio Piccinelli[1*]

[1] Luminescent Materials Laboratory, DB, University of Verona, and INSTM, UdR Verona, Strada Le Grazie 15, 37134 Verona, Italy
[2] Department of Chemistry, Life Sciences and Environmental Sustainability, Parma University, Parco Area delle Scienze, 17/a – 43124, Parma, Italy
[3] Department of Chemistry "G. Ciamician", University of Bologna, via Gobetti 85 – 40129, Bologna, Italy
[4] Center for Chemical Catalysis - C3, Alma Mater Studiorum - Università di Bologna, via Gobetti 85, 40129, Bologna, Italy
[5] Physics Department and CICECO – Aveiro Institute of Materials, University of Aveiro, 3810-193, Aveiro, Portugal
[6] Dipartimento Politecnico di Ingegneria e Architettura, Laboratorio di Tecnologie Chimiche, Università di Udine, via Cotonificio 108, 33100 Udine, Italy
[7] Department of Chemistry and Industrial Chemistry, University of Pisa, via Moruzzi 13, 56124 Pisa, Italy

*corresponding authors' email address: fabio.piccinelli@univr.it, lorenzo.dibari@unipi.it and andrea.melchior@uniud.it

Abstract

In this contribution, the synthesis, the Density Functional Theory (DFT) structural characterization and the spectroscopic investigation of chiral and heteroleptic Tb(III) and Eu(III) complexes are presented. These molecules are characterized by two different ligands: the enantiopure N,N′-bis(2-pyridylmethyl)-*trans*-1,2-diaminocyclohexane-N,N′-diacetic acid (H_2bpcd) and a hydroxycoumarin-based ligand bearing different substituents in C(3) position (*i.e.* acetyl group in Coum, ethyl ester in CoumA, secondary and tertiary amide in CoumB and CoumC, respectively). The coumarin ligands exhibited different luminescence sensitization efficiency towards Tb(III) and Eu(III) ions in the related complexes of chemical formula [Ln(bpcd)(Coum)], [Ln(bpcd)(CoumA)], [Ln(bpcd)(CoumB)], [Ln(bpcd)(CoumC)]. Through theoretical calculations of intramolecular energy transfer (IET) processes (ligand-to-metal) in Eu(III) and Tb(III) complexes, along with quantum yield calculations, we provide a reasonable explanation for the observed differences in their luminescent properties. The nature of the coumarin ligand also affects the chiroptical properties of the Tb(III) complexes [*i.e.* Circularly Polarized Luminescence (CPL) and Electronic Circular Dichroism (ECD)].

Introduction

Despite a large number of contributions in the literature concerning the optical and chiroptical properties of trivalent lanthanide-based chiral coordination compounds, these molecules are still strongly attracting many research groups working in the field of luminescent materials with potential biological[1–6] and technological applications, also including the design of organic light-emitting diodes (OLEDs) emitting circularly polarized (CP) light.[7–19] For these applications, large values of the Circularly Polarized Luminescence brightness (B_{CPL}) factor,[20] are sought and big efforts are still lavished to obtain highly efficient chiroptical complexes of lanthanide(III) exhibiting strong optical signals amenable to CPL measurements and practical applications. High values of molar extinction coefficient (ε), overall quantum yield[21] (Φ_{ovl}), and dissymmetry factor[22] (g_{lum}) contribute to providing high B_{CPL}. Ln(III)-based CPL has some unique and ideal features, which can make it easier to obtain luminescence possessing a very high level of polarization, closer to the highest possible value of g_{lum} (g_{lum} = 2 max.), if compared to common chiral organic molecules. This is because the quantity which governs the CPL activity of a transition $i \rightarrow j$, is its rotational strength R_{ij}, that is the imaginary part of the dot product $R_{ij} = \Im\{\boldsymbol{\mu}_{ij} \cdot \boldsymbol{m}_{ji}\}$ between the electric, $\boldsymbol{\mu}_{ij}$, and magnetic, $\boldsymbol{m}_{ji}$, transition dipoles and it is proportional to the difference of intensity of left (I^L) vs. right (I^R) CP-light emitted. Whilst the most prominent electronic transitions of organic molecules often have only a relatively small magnetic dipole (compared to the electric one), in suitable environments Ln(III) may couple with ligand (induced) electric dipoles, so that the emitted light can gain a sizeable rotational strength.[23] The largest g_{lum} for a particular system is always reached when $|\boldsymbol{\mu}_{ij}| = |\boldsymbol{m}_{ji}|$. Sizeable values of both ε and Φ_{ovl} are usually obtained thanks to the employment of chromophoric ligands capable of both strongly absorbing the exciting radiation (usually in the UV spectral region) and to efficiently transfer excitation to a suitable accepting excited level of the lanthanide ion (*antenna* effect). Finally, it is also important to verify that the emitting level of these ions is not depopulated by the Multiphonon Relaxation Process (MRP)[24] or other non-radiative mechanisms. Some of us recently published a paper in which the Tb(III) luminescence can be efficiently sensitized employing hydroxycoumarin-based *antenna* (Coum, in Figure 1; Φ_{ovl} around 55%) while the required light circular polarization at 546 nm is triggered by the enantiopure N,N′-bis(2-pyridylmethyl)-trans-1,2-diaminocyclohexane-N,N′-diacetic acid (H_2bpcd) ligand.[23,25]

In the present contribution, we investigated the optical and chiroptical properties of a new family of heteroleptic Eu(III) and Tb(III) complexes containing the bpcd ligand and three different hydroxycoumarin-based analogs of the already studied Coum ligand (Figure 1).[25] The coumarins

differ by the nature of the substituent in C(3) position. This substituent is an ester moiety in CoumA,

a secondary or tertiary amide, in the case of CoumB or CoumC, respectively (Figure 1). These structural differences are reflected in the different spectroscopic behaviour of the related complexes (*i.e.* a different efficiency of the *antenna* effect towards the metal ions). Also, the impact of the different substituents on the chiroptical properties of the Tb(III) complexes has been evaluated.

Finally, the most stable structures in methanol solution for each complex have been obtained by means of time-dependent DFT (TD-DFT) calculations, also considering possible isomerism due to the presence of stereogenic sp^3 nitrogen atoms in the bpcd molecule. Additionally, the rates of all possible ligand-to-metal energy transfer channels have been theoretically evaluated, alongside a rate equations model to obtain the quantum yield, to provide a deeper understanding of the different sensitization efficiencies observed across the family of coumarin *antennae*.

Experimental section

$EuCl_3 \cdot 6H_2O$ and $TbCl_3 \cdot 6H_2O$ (Aldrich, 98%), $GdCl_3 \cdot 6H_2O$ (Aldrich, 99.99%) and 2-thenoyltrifluoroacetyl-acetone (Htta, Alfa aesar, 98%) were stored under vacuum for several days at 80°C and then transferred in a glove box.

Both the enantiomers of *N*,*N*′-bis(2-pyridylmethyl)-*trans*-1,2-diaminocyclohexane-*N*,*N*′-diacetic acid (H_2bpcd) ligand, in the form of trifluoroacetate salt, were synthesized as previously reported in the literature.[26] Coum ligand precursor was synthesized as previously reported in the literature.[25]

ESI-MS. Electrospray ionization mass spectra (ESI-MS) were recorded in methanol solutions on a Waters Micromass ZQ 4000 operating in positive ion mode. Experimental conditions: 3.53 kV ES-probe voltage, 20 V cone potential, 200 L h^{-1} flow of N_2 spray-gas, incoming-solution flow 20 μL min^{-1}.

The synthesis and characterization of the other coumarin ligands are reported in the Supporting Information file (pages S2-S12).

The complexes have been synthesized as follows:

At room temperature, $EuCl_3 \cdot 6H_2O$ (0.057 g, 0.16 mmol, 1 equiv.), or $TbCl_3 \cdot 6H_2O$ (0.058 g, 0.16 mmol, 1 equv.) or $GdCl_3 \cdot 6H_2O$ (0.058 g, 0.16 mmol, 1 equiv.) was added to a previously prepared methanol solution containing KOH (0.035 g, 0.62 mmol, 4 equiv.) and H_2bpcd (*S,S* or *R,R*) (0.100 g, 0.16 mmol, 1 equiv., as trifluoroacetate salt). In another flask, 1 equiv. of Coumarin [(A 0.037 g; B 0.034 g; C 0.041 g), 0.16 mmol)] was solubilized in methanol and added to a solution of NaOMe [for

Coumarin A and C(0.011 g, 0.16 mmol, 1 equiv.)] or NaOEt [for Coumarin B (0.008 g, 0.16 mmol, 1 equiv.)], in the same solvent (10 mL). The deprotonated Coumarin (A, B or C) ligand was slowly added to the solution containing the Ln(III) complex. The final mixture was stirred at room temperature for 2 h. Then, the solvent was removed under reduced pressure, and the desired product was obtained as a yellow powder upon extraction in dichloromethane (8 × 3 mL) followed by solvent removal in vacuo. All the products were obtained with yields in the 91-93% range.

Luminescence and decay kinetics. Room temperature luminescence was measured with a Fluorolog 3 (Horiba-Jobin Yvon) spectrofluorometer, equipped with a Xe lamp, a double excitation monochromator, a single emission monochromator (mod. HR320), and a photomultiplier in photon counting mode for the detection of the emitted signal. All the spectra were corrected for the spectral distortions of the setup. The spectra in solution were recorded on methanol (50 μM) solutions.

In decay kinetics measurements, a Xenon microsecond flashlamp was used and the signal was recorded through the multichannel scaling method. True decay times were obtained using the convolution of the instrumental response function with an exponential function and the least-square-sum-based fitting program (SpectraSolve software package). Low temperature (77 K) luminescence and decay kinetics of the Ln(III) excited states were measured with an Edinburgh FLS1000 spectrofluorometer equipped with both continuous and pulsed Xe lamp, a double excitation monochromator, a single emission monochromator and a photomultiplier in photon counting mode for the detection of the emitted signal.

Circularly Polarized Luminescence. CPL spectra were recorded with the homemade spectrofluoropolarimeter described previously.[27] The measurements were carried out in 1 mM methanol solutions. All samples were irradiated at 254 nm in a 1 cm semi-micro (aperture 4 mm) optical glass cells using the following parameters: scan speed 0.5 nm/sec, integration time 2 sec, photomultiplier tube driving voltage 500 V, accumulations 4.

Electronic Circular Dichroism. ECD spectra were recorded with a Jasco J1500 spectropolarimeter on CH_3OH 1 mM solutions in a 0.02 cm-cell.

Overall quantum yield measurements. Overall quantum yields were measured by adopting the relative method. Fluoresceine in NaOH 0.1M (fluorescence quantum yield: 0.9) was used as standard. Absorption spectra were collected with a Perkin Elmer Lambda 650 UV-Vis spectrophotometer. Emission spectra were recorded with an Edinburgh FLS1000 fluorometer and were corrected for the

excitation intensity and the detector sensitivity. The samples were dissolved in methanol, keeping their absorbance lower than 0.1. Within the instrumental error (±10%), we obtained the same values of overall quantum yield for the two enantiomers.

Theoretical section

DFT calculations. All molecular structures of the complexes were obtained utilizing DFT calculations run in Gaussian 16 (version A.03).[28] In previous works[5,25,26,29,30] the paramagnetic Eu(III) ion was replaced by Y(III) which is a suitable substitute. This choice is also supported by the isostructural complexes found with analogous hexa-dentate ligands EDTA and CDTA. In the crystal structures with the latter two ligands,[31–33] Y(III) and Eu(III) ions are 9-coordinated with EDTA (ligand and 3 water molecules bound to the metal) and 8-coordinated with CDTA (2 bound waters). Since Y(III) has a smaller ionic radius than Eu(III) and Tb(III), also the calculations for the same complexes with the larger La(III) ion were carried out. To determine the solvent molecules bound to the complexes, also the geometries of [Ln(bpcd)(Coum)]·4H_2O (with L = Y, La), where water molecules replaced methanol, were considered.

The functional B3LYP[34,35] was used with the 6-31+G(d) basis set for all ligand atoms and MWB28 pseudopotential and valence electrons basis set for the metal ions.[36,37] Geometry optimizations were carried out at the DFT level with a polarizable continuum model (PCM) to simulate solvation.[38]

As in a previous work,[39] the excited states (T_1 and S_1) energies were obtained employing the time-dependent DFT approach (TD-DFT) on the [Y(bpcd)L] complexes using the same level of theory as in the geometry optimizations, as it was shown that B3LYP functional provides good prediction of UV-Vis spectra of coumarin derivatives.[40]

Intramolecular energy transfer calculations. The energy transfer rates for [Ln(bpcd)CoumA·H_2O] and [Ln(bpcd)CoumB·H_2O], where Ln = Eu^{3+} and Tb^{3+}, were calculated according to the procedures described previously.[41] With the help of the TD-DFT results, the donor state of the ligand can be localized and the donor-acceptor distances (R_L in Å) can be properly calculated through Eqs. S3–S5 (see Supporting Information). The JOYSpectra web platform (http://joyspectra.website) was employed to perform the calculations.[42]

Multiphonon rates. The multiphonon decay rates (W_{mp}) between adjacent Ln(III) states were estimated using the Miyakawa-Dexter model (Eq. S9) within the framework of the Energy Gap Law (Eq. S8).[43,44]

Rate equations model and overall quantum yield calculations. The rates of all possible ligand-to-metal energy transfers, multiphonon processes, and lifetimes were incorporated into a rate equations model (Eqs. S10–S14), following the procedure outlined in reference 45. This model was implemented in Python, and the code is provided in the Supporting Information. The theoretical overall quantum yield was then evaluated from the steady-state populations of the emitting and ground levels (Eq. S16).

Results and discussion

Synthesis and DFT structure of the complexes

Both enantiomers (*S,S* or *R,R*) of [Ln(bpcd)(CoumA)], [Ln(bpcd)(CoumB)], and [Ln(bpcd)(CoumC)] complexes (Figure 1) have been obtained in very high chemical yields and high degrees of purity, as confirmed by ESI-MS data (Figures S1-S3).

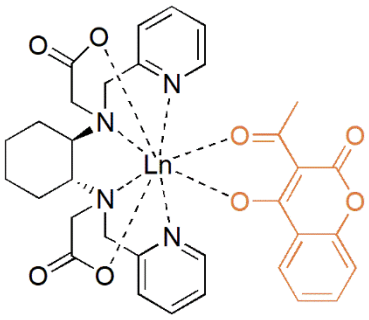

[Ln(bpcd)(**Coum**)]
Eu (yield 95%)
Tb (yield 95%)
Gd (yield 90%)

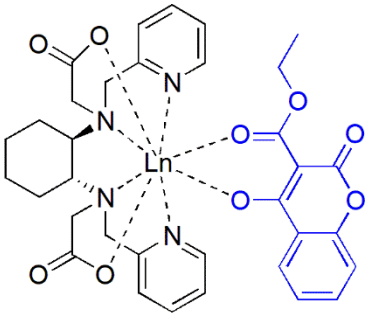

[Ln(bpcd)(**coumA**)]
Eu (yield 93%)
Tb (yield 95%)
Gd (yield 82%)

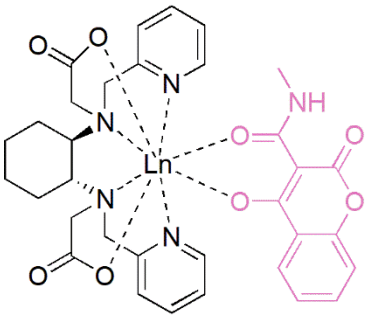

[Ln(bpcd)(**coumB**)]
Eu (yield 91%)
Tb (yield 93%)
Gd (yield 84%)

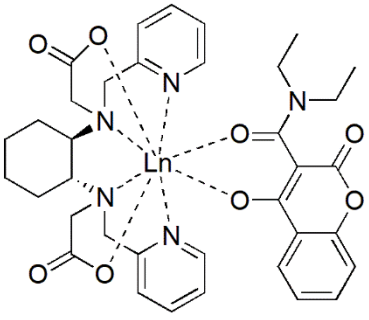

[Ln(bpcd)(**coumC**)]
Eu (yield 97%)
Tb (yield 92%)
Gd (yield 88%)

Figure 1. Ln(III) complexes discussed in this work. The *R,R* enantiomers are shown for all, but both enantiomers are considered in this work.

DFT calculations have been carried out to obtain structural information on the [Ln(bpcd)L] (**L** = Coum, CoumA-C) complexes by studying the diamagnetic Y(III) and La(III) analogues of the Eu/Tb complexes. As previously pointed out,[25] several isomeric forms can be present, depending on the arrangement of the pyridine and acetate groups in bpcd ligand (*trans*-O,O, *trans*-N,N and *cis*-OO,NN). These isomers hosting the CoumA and CoumB ligands (Figure 2) present a negligible difference in energy ($\Delta E < 0.6$ kcal mol^{-1}), so a mixture should be present in solution. In the case of the [Y(bpcd)(CoumC)] complex, the *trans*-NN and *cis*-OO,NN isomers result in ~1.5 kcal mol^{-1} lower in energy than the *trans*-O,O one, likely due to the presence of the bulky diethylamino- group. The calculated number of coordinated methanol molecules (*vide infra*) is 1.2, 0.7 and 0.6 for Tb(III) which has an ionic radius more similar to the Y(III) model compound. In our previous work[25] the [Y(bpcd)(Coum)]·4H_2O complexes discarded the coordination of water to the metal ion. Moreover, it was shown that in the [La(bpcd)(Coum)] 4H_2O structures, the trans-OO and trans-NN isomers can bind two water molecules, while only one is observed in the cis-OO,NN one. Here, again it appears that La(III) complexes can accommodate one or two water molecules as shown in Figure S4. This result is in agreement with the higher number of methanol molecules found for Eu (1.3, 1.1, 1.5 and 1.2 for Coum and CoumA-C respectively, see Table 2) with respect to Tb (0.7, 1.2, 0.7 and 0.6), accounting for the slightly bigger ionic radius of the former ion.

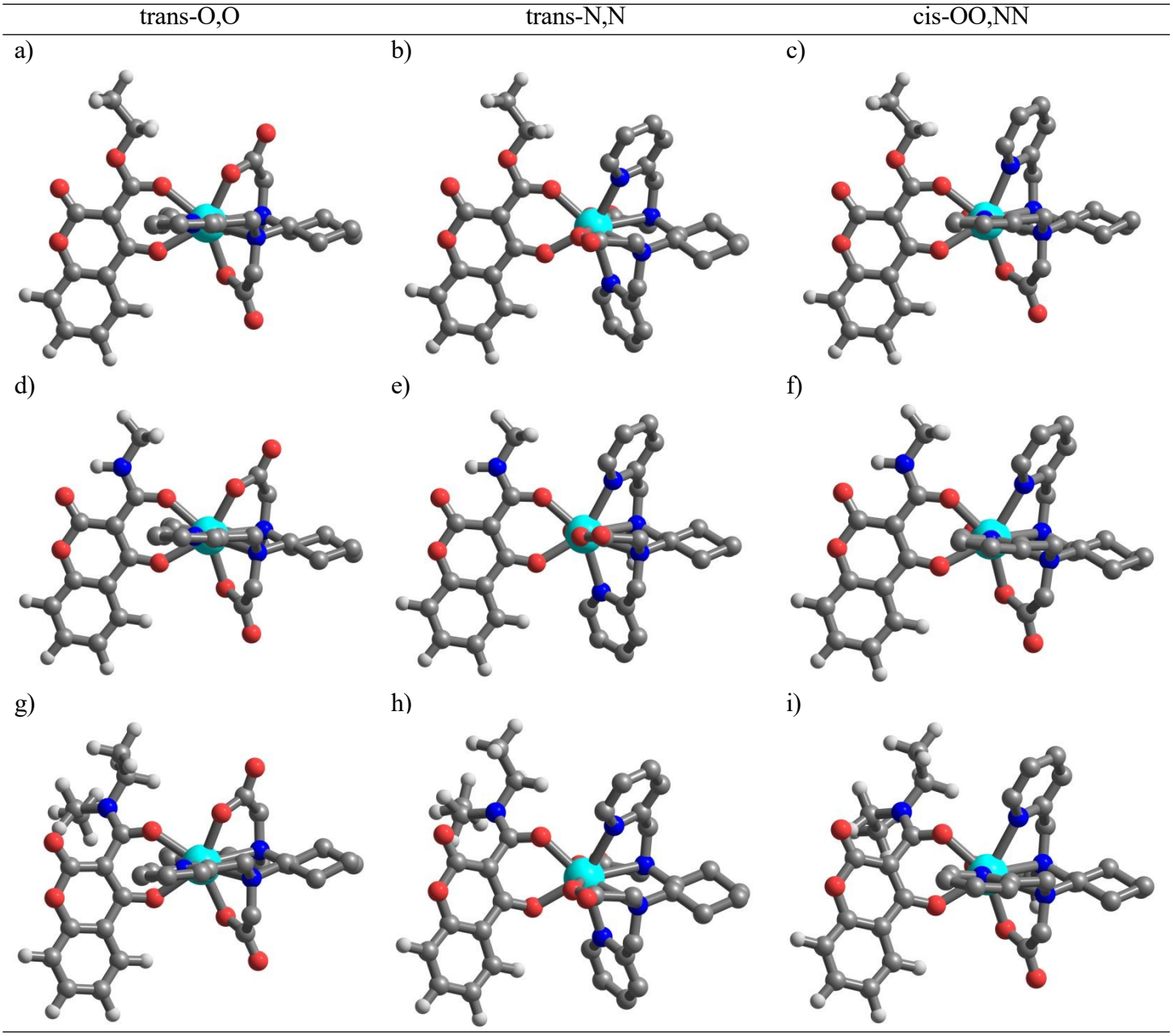

Figure 2. Minimum energy structures of the isomers of the [Y(bpcd)(CoumA)] (a-c), [Y(bpcd)(CoumB)] (d-f) and [Y(bpcd)(CoumC)] (g-i) complexes obtained from DFT calculations. Hydrogen atoms of the $Y(bpcd)^{+}$ moiety are hidden for clarity.

Spectroscopic characterization

S_1 and T_1 energy positions of the coumarins

To determine the position of the main singlet and triplet excited states of the coumarin ligands (S_1 and T_1), we collected the RT absorption and the 77 K emission spectra of the four Gd(III)-based complexes (Figure 3). The relative energy position of the aforementioned states has been determined employing the tangent method on the above discussed spectra, that allows to obtain the $S_0 \rightarrow S_1$ and $T_1 \rightarrow S_0$ zero-phonon transition energies. The position of the triplet and singlet excited states for the family of coumarin ligands are around 30000 and 26000 cm^{-1}, respectively (Table 1). As previously demonstrated by some of us, at higher energy (close to 37000 cm^{-1}), an additional electronic transition involving the molecular orbitals localized on bpcd ligand can be exploited to sensitize the Eu(III)[39] and Tb(III)[26] luminescence (not discussed here).

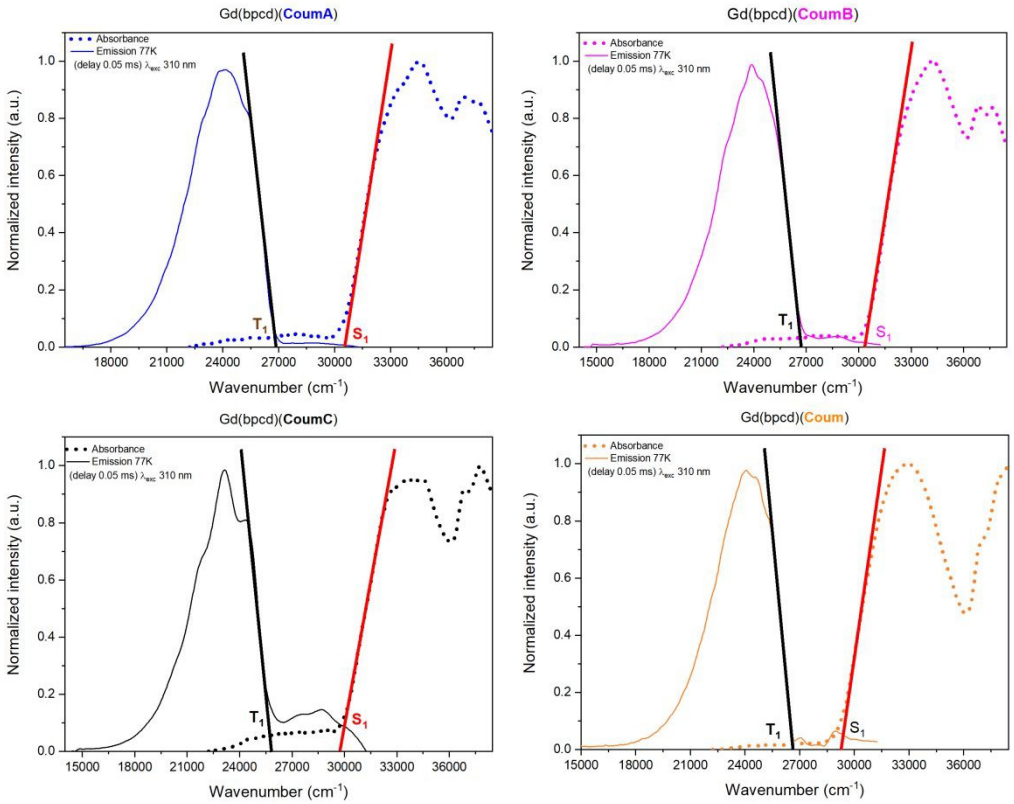

Figure 3. RT absorption spectra in methanol (50 μM) (dotted lines) and 77 K phosphorescence spectra in organic glass (EtOH/MeOH = 4:1) (solid lines) of [Gd(bpcd)(Coum*); Coum* = Coum, CoumA, CoumB and CoumC].

Even though only small differences in the position of S_1 and T_1 are observed, we can see a regular increase of the $\Delta(S_1- T_1)$ energy gap, passing from Coum (2660 cm^{-1}) to Coum C (3804 cm^{-1}) (Table 1 and Fig.S5). We also determined the triplet state lifetime upon collection at 77K of the luminescence decay curve at 420 nm (around 24000 cm^{-1}) upon excitation at 310 nm (around 32000 cm^{-1}), in the coumarin main absorption band[25,46] (Figure S6). As the decay curves deviate significantly from the single exponential behavior, the average decay times have been evaluated using the formula reported previously.[47] All the reported lifetimes are in the ms range and therefore compatible with a spin-forbidden $T_1 \rightarrow S_0$ electronic transition. Only [Gd(bpcd)(CoumB)], with a triplet lifetime of around 3.2 ms, shows a significant deviation from the average value of 4 ms (Table 1).

Table 1. Spectroscopic data related to singlet and triplet excited states of the ligands in Gd(III) coumarin-based complexes.

Ligand	**Energy position (cm^{-1})**		**$\Delta(S_1-T_1)$ (cm^{-1})**	**T_1 state lifetime (ms)**
	S_1	**T_1**		
Coum	29287	26627	2660	3.8
CoumA	30487	26863	3624	4.0
CoumB	30360	26695	3665	3.2
CoumC	29766	25962	3804	4.2

Photophysical features and sensitization mechanism

The luminescence excitation and emission spectra of methanol solution (50 μM) of the Tb(III)- and Eu(III)-based complexes under investigation are reported in the Figures 4 and S7. Upon excitation of the coumarin moiety (at 300 nm) the typical *f-f* emission bands stemming from the $^5D_4$ level of Tb(III) and $^5D_0$ level of Eu(III) are observed, indicating the presence of a ligand-to-metal energy transfer (LMET) process for both ions and involving all the coumarins. Do note though that, in the emission spectra of the Eu(III) complexes, a small broad band, attributable to ligand fluorescence, around 400 nm is present. The calculated quantum yield related to the ligand fluorescence upon excitation at 300 nm are lower than 1% {0.4% for [Eu(bpcd)(CoumA)], 0.5% for [Eu(bpcd)(CoumB)], 0.7% for [Eu(bpcd)(CoumC)] and non-detectable for [Eu(bpcd)(Coum)}.

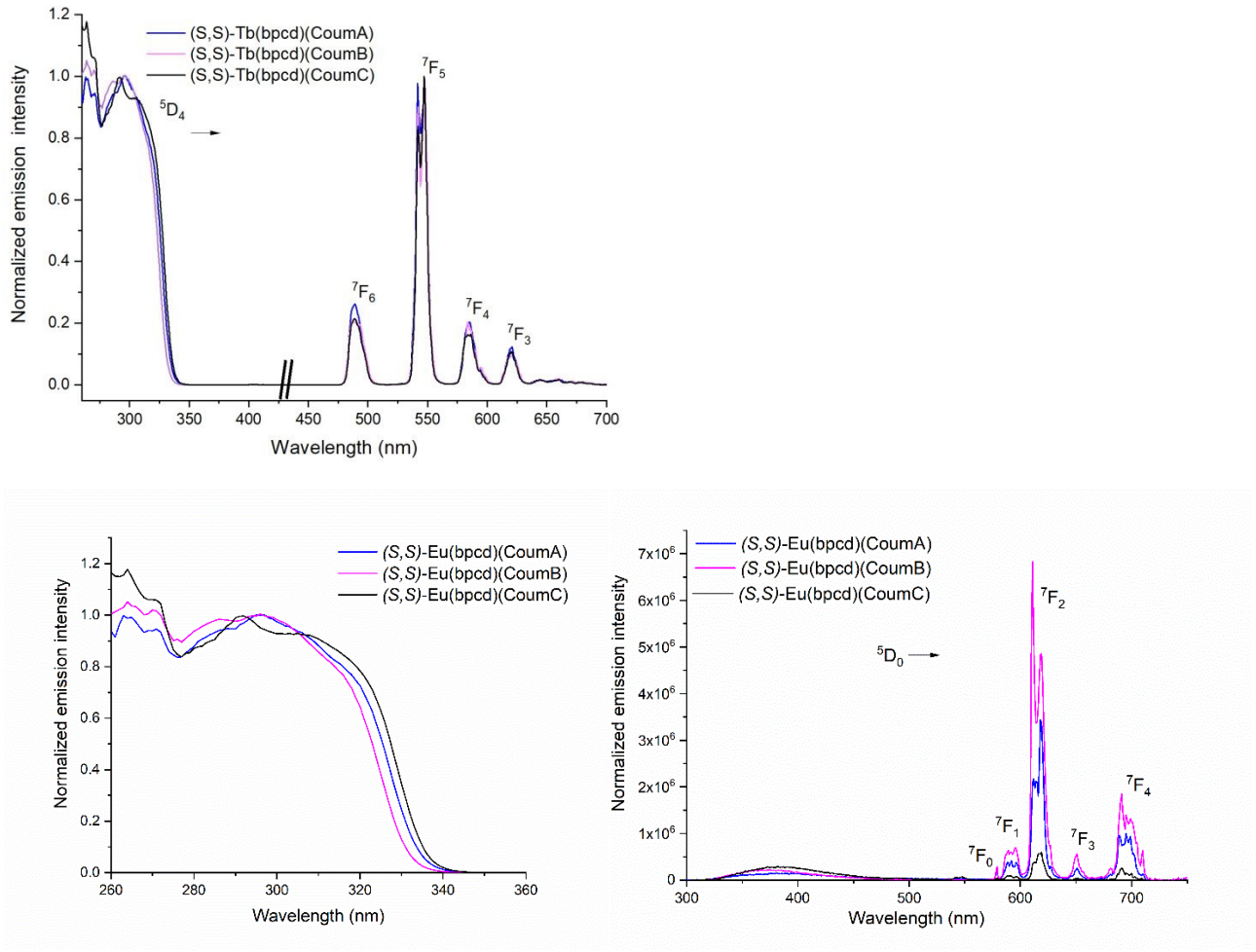

Figure 4. Room temperature excitation (left, λ_{em} = 546 nm) and emission spectra (right, λ_{exc} = 300 nm) of (*S*,*S*) Tb(III)-based complexes in methanol solution (6 μM) (up) and room temperature excitation (left, λ_{em} = 614 nm) and emission spectra (right, λ_{exc} = 300 nm) of Eu(III)-based complexes in methanol solution (6 μM) (bottom). The emission spectra of the Eu(III) complexes are normalized to the value of the absorbance of the solutions at 295 nm (lower than 0.1).

The most relevant photophysical properties of the complexes are measured also in deuterated methanol and are collected in Table 2. Based on the Judd-Ofelt theory,[48] the estimation of τ_{rad} is directly feasible only in the case of Eu(III) ion[49,50] and therefore the Φ_{Ln}, which is equal to τ_{obs}/τ_{rad}, can be reported only for it. Analogously, since the efficiency of the sensitization of the Ln(III) luminescence (η_{sens}) is equal to Φ_{ovl}/Φ_{Ln} we can report in the table the precise values of η_{sens} only for the Eu(III)-based complexes. As for the Tb(III) complexes however, considering that Φ_{ovl} is always $\leq \Phi_{Ln}$, and therefore $\eta_{sens} \geq \Phi_{ovl,}$ we report in the table 2 a range of possible η_{sens} values (7th column of Table 2).

Table 2. Main photophysical data for the complexes under investigation dissolved in methanol (50 μM). τ_{obs} is the observed lifetime, τ_{rad} is the radiative lifetime, *m* is the number of methanol molecules in the inner coordination sphere, Φ_{Ln} is the intrinsic quantum yield, Φ_{ovl} is the overall quantum yield considering Ln(III) emission only and η_{sens} (Φ_{ovl}/Φ_{Ln}) is the sensitization efficiency of the *antenna*.[a] in CH_3OH, [b] in CD_3OD.

Coumarin	Complex	τ_{obs} (ms)	τ_{rad} (ms)	*m*	Φ_{Ln}(%)	η_{sens}(%)	Φ_{ovl}(%)
Coum	[Tb(bpcd)(Coum)]	1.42(1)[a]		0.7		53-100[a]	53[a]
		1.59(1)[b]				65-100[b]	65[b]
	[Eu(bpcd)(Coum)]	0.80(1)[a]	2.42(1)[a]	1.3	33[a]	21[a]	7[a]
		1.40(1)[b]	2.41(3)[b]		58[b]	19[b]	11[b]
Coum A	[Tb(bpcd)(CoumA)]	1.60(1)[a]		1.2		35-100[a]	35[a]
		2.07(1)[b]				47-100[b]	47[b]
	[Eu(bpcd)(CoumA)]	0.82(1)[a]	2.47(7)[a]	1.1	33[a]	6[a]	2[a]
		1.44(1)[b]	2.54(3)[b]		57[b]	5[b]	3[b]
Coum B	[Tb(bpcd)(CoumB)]	1.75(1)[a]		0.7		62-100[a]	62[a]
		2.05(1)[b]				77-100[b]	77[b]
	[Eu(bpcd)(CoumB)]	0.71(1)[a]	2.43(1)[a]	1.5	29[a]	7[a]	2[a]
		1.48(1)[b]	2.37(9)[b]		62[b]	8[b]	5[b]
Coum C	[Tb(bpcd)(CoumC)]	1.80(1)[a]		0.6		26-100[a]	26[a]
		2.08(1)[b]				33-100[b]	33[b]
	[Eu(bpcd)(CoumC)]	0.79(1)[a]	2.75(6)[a]	1.2	29[a]	1[a]	<1[a]
		1.40(1)[b]	2.70(7)[b]		52[b]	1[b]	<1[b]

By measuring the observed lifetimes in methanol (τ_{MeOH}) and deuterated methanol (τ_{CD3OD}), it is possible to determine the number of solvent molecules in the proximity of the metal ion (*m*) by means of the equation reported in the literature[51] [$m = 2.1(1/\tau_{MeOH} - 1/\tau_{CD3OD})$ for Eu(III) and $m = 8.4(1/\tau_{MeOH} - 1/\tau_{CD3OD})$ adapted for Tb(III)]. Interestingly, the experimental *m* clearly decreases from Eu (1.3-1.5) to Tb (0.6-0.7) in the case of complexes containing Coum; CoumB and CoumC. As already documented[25] this evidence agrees with the hypothesis that small changes in ionic radius here (Tb(III) is slightly smaller than Eu(III)) determine a different number of coordinated solvent molecules in the

complex. On the contrary, in the case of CoumA-based complexes, there is no change in the value of *m* (around 1) upon changing the metal ion.

Despite the similar core structure of the coumarins *antennae,* the different substituents in the lateral chain significantly affect the values of the Φ_{ovl}. Firstly, all coumarins better sensitize the Tb(III) luminescence than the one of Eu(III). In addition, the best *antenna* for Tb(III) is represented by the secondary amide CoumB (η_{sens} not lower than 62% in methanol), whilst the tertiary amide CoumC is the worst one (η_{sens} not lower than 26% in methanol).

While the Tb(III) compounds exhibit moderate to high Φ_{ovl}, the Eu(III) analogues show very low values. One potential explanation for this discrepancy could be the presence of a ligand-to-metal charge transfer (LMCT) state, which might interrupt the sensitization process and lead to luminescence quenching in Eu(III) compounds.[52] However, our analysis revealed that no LMCT band was detectable in the spectra.[25] Experiments supported this conclusion: *i*) the Φ_{ovl} of fluorescence for Gd(III) complexes were found to be comparable to those of Eu(III) complexes, albeit at very low levels ([Ln(bpcd)(CoumA)]: Φ_{ovl} = 0.4% for Eu(III) and Φ_{ovl} = 0.7% for Gd(III); [Ln(bpcd)(CoumB)]: Φ_{ovl} = 0.5% for Eu(III) and Φ_{ovl} = 1% for Gd(III); [Ln(bpcd)(CoumC)]: Φ_{ovl} = 0.7% for Eu(III) and Φ_{ovl} = 1.4% for Gd(III)); *ii*) the absorption spectra in the UV range of Gd(III) and Eu(III)-based complexes are fully superimposable.

Additionally, the fluorescence lifetimes of the ligand for both Gd(III) and Eu(III) complexes were similar, falling within the nanosecond range, although we approached the instrumental limits for decay curve collection. Notably, the fluorescence peak profiles were identical for both Gd(III) and Eu(III) complexes. The expected impact of an LMCT band near the S_1 state of coumarin ligands would significantly alter the fluorescence decay for Eu(III), but this was not observed. Furthermore, while the fluorescence quantum yields should theoretically be affected by the presence of an LMCT state, the differences between Gd(III) and Eu(III) remain minimal. Finally, it is important to note that the strong phosphorescence observed at 77 K for Gd(III) complexes is entirely absent at room temperature.

In order to understand the reasons beyond the different sensitization efficiency of the family of coumarin *antennae*, according to the procedures described previously,[39,41] we calculated the energy transfer rates of Eu(III) and Tb(III) complexes containing two coumarins which significantly differ by the sensitization efficiency (*i.e.* CoumA and CoumB, chosen as representative). Even if in the case of [Tb(bpcd)(CoumB)] we determined a number of coordinating solvent molecules slightly lower than one, in the calculations we decided to consider one coordinating solvent molecule for each investigated complex (here water is used to model methanol). Furthermore, to simplify the computational model, only the minimum energy structures of the *trans*-N,N isomer of the La(III)-based counterparts are taken into account.

Figure S13 shows the molecular orbitals (MOs) compositions associated with the first triplet (T_1) and first singlet (S_1) for La(III) analogs. It can be noted that both S_1 and T_1 states (see unoccupied MOs) are spread through the CoumA and CoumB ligands, being these ligands responsible for the ligand-to-Ln energy transfer processes. Among all transitions, the S_1 state of [La(bpcd)(CoumB)] H_2O is the only one characterized by an electronic charge displacement. This transition brings the charge spread in the whole organic ligands (including the bpcd molecule) to a more confined part in the CoumB ligand. This may be the reason behind the rising of the calculated S_1 energy for CoumB-based complex (34000 cm^{-1}). Such a difference between the calculated and experimentally determined energy positions of T_1 and S_1 (compare data in Table 1 and Figure S13) can be attributed to the absence of intermolecular interactions in the DFT/TD-DFT calculations. Generally, intermolecular interactions can cause the electronic density of a molecule to spread more among molecules, resulting in lower energy for the excited states.

This explanation justifies the observed energy differences and, more importantly, helps us to understand where the S_1 and T_1 states are spatially localized throughout the ligands in a single molecule, allowing us to extract the donor-acceptor distance from the TD-DFT calculation.

Once we have the compositions of molecular orbitals (MOs), we can determine the donor-acceptor distance (R_L)[53] as illustrated in Figure S14. In the case of the CoumA compound, the centroid of the MOs for the S_1 and T_1 states coincides, resulting in $R_L \approx 4.66$ Å (Figure S14a). On the other hand, CoumB exhibits a shorter R_L compared to CoumA, and there is a slight difference between the S_1 and T_1 states, with R_L values of approximately 4.58 Å and 4.64 Å, respectively. In this context, it is important to note that: i) the energy transfer rate dies off with donor-acceptor distance and ii) the energy transfer rate is dependent on the nature of the D-A energy transfer mechanism, in other words, the dipole-dipole (W_{d-d}, Eq. S3), dipole-multipole (W_{d-m}, Eq. S4) and exchange (W_{ex}, Eq. S5) mechanisms. Regardless of the nature of the energy transfer mechanism, the estimated R_L values for the complexes containing CoumA and CoumB suggest a higher energy transfer rate in the case of the latter complexes, in agreement with the higher η_{sens} for CoumB-based complexes (Table 2).

The energy transfer rates were quantified through the JOYSpectra web platform (http://joyspectra.website)[42] and more details on the calculations of energy transfer in lanthanide chelates can be found in ref. [41]. Our analyses are based on the diagrams in Figure 5, where W^S and W^T indicate the forward energy transfer channel from the S_1 and T_1, respectively. The $W^{T'}$ is the energy transfer rates from the T_1 to the main emitting levels of Ln^{3+} [*i.e.*, $^5D_0$ for Eu(III) and $^5D_4$ for Tb(III)]. This distinction is useful for a clearer picture of the population of the emitting levels. All the

Ln-to-ligand backward energy transfer rates are indicated by a subscript *b*.

By analyzing the energy transfer rates in different channels (S_1 and T_1) and involving various pathways (Tables S1 – S8), it can be observed that the backward energy transfer from the emitting levels ($W_b^{T'}$) is insignificant for all the complexes (Figure 5c, f). This is advantageous for emission since backward energy transfer, particularly involving emitting levels, can act as a significant emission quenching channel. Moreover, the direct energy transfer rates to the emitting level ($W^{T'}$) are slightly higher for Tb(III) compounds (1.1×10^7 and 1.4×10^7 s^{-1} for CoumA and CoumB, respectively). This is because the T_1 state of CoumA and CoumB is in a more resonant energy condition with the Tb(III) $^5D_4$ level (Δ = 3769 and 3479 cm^{-1}, respectively) compared to the Eu(III) $^5D_0$ level (Δ = 6920 and 6630 cm^{-1}, respectively). In addition, the [Tb(bpcd)CoumB·H_2O] complex exhibits the highest $W^{T'}$ value and is the only one where the condition $W^{T'} > W^{T}$ is met among all the complexes. This indicates that energy transfer preferably flows directly from the ligand's T_1 state to the Tb(III) emitting level ($T_1 \rightarrow {}^5D_4$), rather than transferring to higher states and potentially losing energy in the process. This condition may favour a better quantum yield, as corroborated by the highest value observed among all complexes (Table 2).

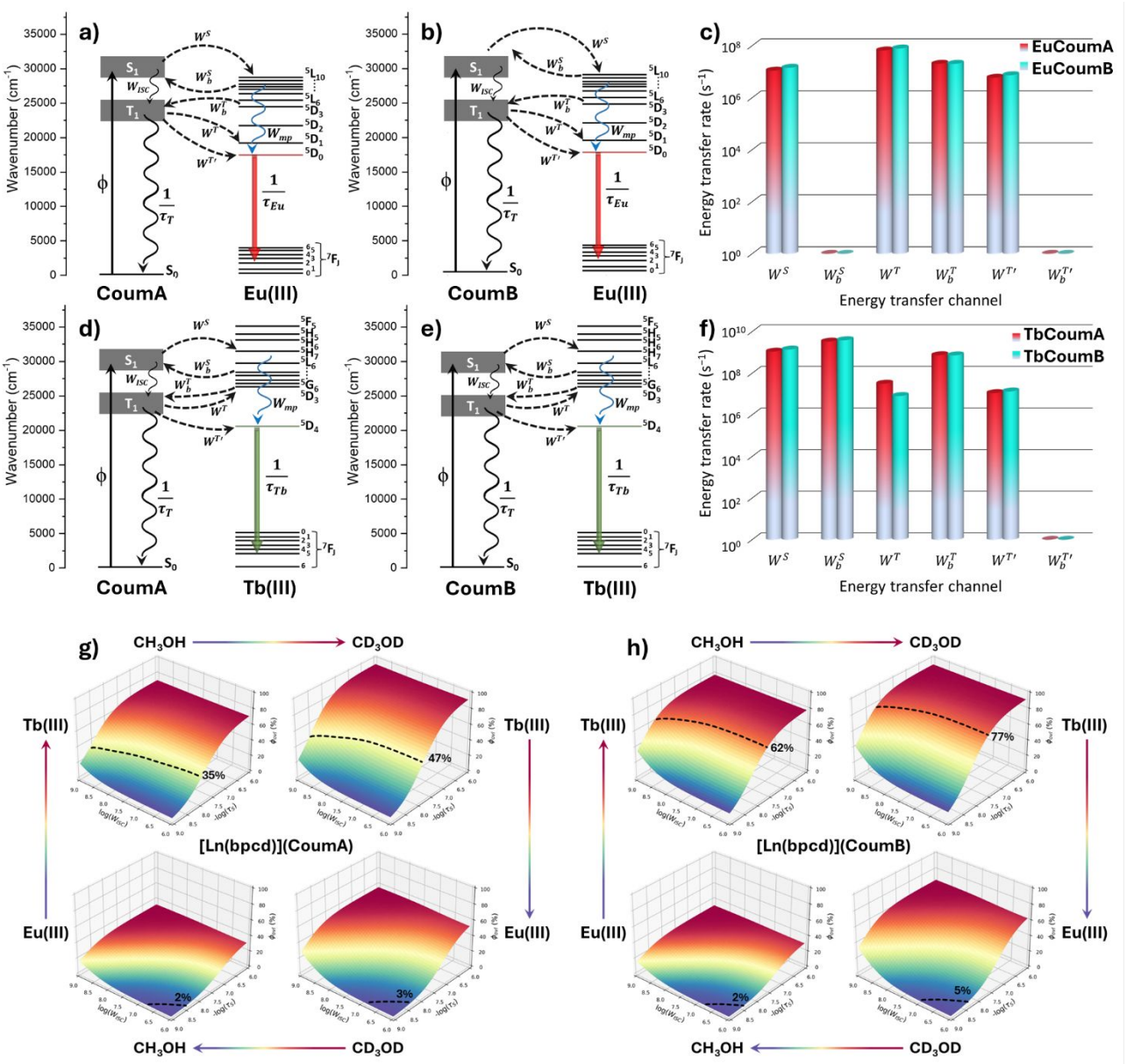

Figure 5. Jablonski-type energy levels diagrams for (a,b) Eu(III) and (d,e) Tb(III) Coumarin-based compounds. (c,f) Energy transfer rates for the different channels considered, as illustrated in the diagrams. Theoretical overall quantum yields (Φ_{ovl} in %) as a function of log(W_{ISC}) and —log(τ_S) for (g) [Ln(bpcd)CoumA·H_2O] and (h) [Ln(bpcd)CoumB·H_2O] compounds (Ln: Eu and Tb). The estimations of ϕ_{ovl} in CH_3OH and CD_3OD solvents are considered in the rate equations model by using the values of the τ_{obs} and $A_{rad} = 1/\tau_{rad}$ in Table 2. The dashed lines are guides for the eye, representing the measured Φ_{ovl}.

W^S and W_b^S are not negligible for all the complexes and are above 10^9 s^{-1} for the Tb(III)-Coumarins. What is quite remarkable is the difference in the energy transfer rates of the channels involving the S_1 states of CoumA and CoumB. High rates of forward energy transfer channel are found for Tb(III) ion, in particular in the case of CoumB (W^S = 1.39×10^9 s^{-1}). This is in agreement with what is

described in the literature in which the sensitization through the S_1 state is commonly observed for Tb(III) compounds[54–56] whilst it is rare for Eu(III).[57,58] This difference can be mainly attributed to the Tb(III) $^7F_6 \rightarrow {}^5G_6$ (~26423 cm^{-1}) and $^7F_5 \rightarrow {}^5G_5$ (~25719 cm^{-1}) transitions, which involve a strong participation of the exchange mechanism due to their higher squared spin matrix elements, $\langle {}^7F_6 \| S \| {}^5G_6 \rangle^2 = 0.555$ and $\langle {}^7F_5 \| S \| {}^5G_5 \rangle^2 = 0.243$.[54] The energy transfer pathways $[S_1 \rightarrow S_0] \rightarrow$Tb(III)$[{}^7F_6 \rightarrow {}^5G_6]$ (pathway #3 in Tables S5 and S7) and $[S_1 \rightarrow S_0] \rightarrow$Tb(III)$[{}^7F_5 \rightarrow {}^5G_5]$ (pathway #25 in Tables S5 and S7) are predominant in the total IET rate involving the transfer from S_1 state for Tb(III)-Coumarin based complexes, contributing more than 59% and 23% to the total W^S rate, respectively. In these pathways, the major contributions follow the order $W_{ex} > W_{d-m} > W_{d-d}$, indicating the dominance of exchange and dipole-multipole mechanisms over dipole-dipole interactions. Concerning the backward W_b^S rate, the main pathways are Tb$[{}^5H_5 \rightarrow {}^7F_5] \rightarrow [S_0 \rightarrow S_1]$, Tb$[{}^5H_4 \rightarrow {}^7F_5] \rightarrow [S_0 \rightarrow S_1]$, Tb$[{}^5F_5 \rightarrow {}^7F_5] \rightarrow [S_0 \rightarrow S_1]$, and Tb$[{}^5F_4 \rightarrow {}^7F_5] \rightarrow [S_0 \rightarrow S_1]$ (pathways #33, #34, #35, and #36 in Tables S6 and S8) with respective contributions to the total W_b^S around 10.5%, 27.0%, 11.4%, and 38.0%. These pathways are dominated only by W_{ex} mechanism.

Concerning Eu(III) compounds, it is evident that the backward energy transfer W_b^S is negligible and $W^T > W^S$ for both CoumA and CoumB ligands. The dominant pathway for energy transfer through the T_1 state is overwhelmingly the $[T_1 \rightarrow S_0] \rightarrow$Eu(III)$[{}^7F_0 \rightarrow {}^5D_1]$ one, which accounts for 89.7% of the total T_1 involved rate ($W^T + W^{T'}$) for CoumA (pathway #18 in Table S1) and 89.4% for CoumB (pathway #18 in Table S3). This substantial contribution underscores the role of the $^5D_1$ state in the sensitization process, as discussed in recent literature.[59–61]

Considering a mean phonon energy of $\hbar\bar{\omega}$ = 1700 cm^{-1}, attributed to the C=O stretching mode, and knowing that electron-phonon coupling in lanthanide states leads to small Huang-Rhys factors (typically between 0.02 and 0.10),[62–64] the estimated multiphonon decay rates (Eq. S8) between adjacent levels were 7.26×10^6 s^{-1} for Eu(III) and 7.78×10^6 s^{-1} for Tb(III) ions (Table S9).

Using all estimated rates so far, we calculated the theoretical overall quantum yields (Φ_{ovl}) based on a rate equations model (Eqs. S10–S14),[45] implemented in the Python code provided in the Supporting Information. Since some parameters, such as the intersystem crossing rate (W_{ISC}) and the fluorescence (τ_S) and phosphorescence (τ_T) lifetimes, cannot be easily determined from theory or experiment, we modeled Φ_{ovl} by varying these unknown parameters. For example, the T_1 lifetime (τ_T) at room temperature is expected to be shorter than those obtained from the phosphorescence band at 77 K for the Gd(III) analogue compounds (Table 1), suggesting that τ_T should fall between the ms

and μs range.

Initially, simulations of Φ_{ovl} by varying τ_T (ranging from ms to μs) and W_{ISC} (from 10^6 to 10^9 s^{-1}) was done, as shown in Figure S15. However, Φ_{ovl} proved less sensitive to this range of τ_T because all compounds exhibited $W_T > 1/\tau_T$, particularly for Eu(III) compounds. The inability to fully reproduce the values of Φ_{ovl} for Eu(III) compounds suggests that the main contributions arise from the competition between W_{ISC} (which feeds the T_1 state) and τ_S. Thus, in a second batch of Φ_{ovl} calculations, now varying W_{ISC} and τ_S (from μs to ns) and fixing τ_T at 10 μs, all experimental Φ_{ovl} for [Ln(bpcd)CoumX·H_2O] compounds (Ln = Eu and Tb, X: A and B) were successfully reproduced, as shown in Figure 5g,h. Additionally, common values aligned with the experimental data, suggesting that $W_{ISC} \approx 10^7$ s^{-1}, $\tau_S \approx$ 10 ns, and $\tau_T =$ 10 μs are consistent for both CoumA and CoumB compounds.

Chiroptical spectroscopy (CPL and ECD spectra)

Due to the very low performance of the investigated coumarins as *antennae* for Eu(III), we did not find interesting to investigate the chiroptical features of the Eu(III)-based complexes. For this reason, this section is devoted to the chiroptical characterization of the Tb(III) complexes.
The absorption peaks centred around 230, 300, and 320 nm, present for all the studied coumarins, are related to the electronic transitions of these molecules,[25,46] while the shoulder at 270 nm is due to the absorption of the $bpcd^{2-}$ ligand, as already mentioned.[26]

The UV-ECD spectrum of the Coum-based complex displays only weak or very weak ECD signals associated with the absorption bands listed above (Figure 6, right). The absence of significant features may suggest that the complex exists as a conformational manifold, where the various chromophores occupy enantiotopic positions (neglecting the other stereogenic elements) with almost equal probability. In other words, the observed spectra may be the result of compensation of oppositely signed exciton interactions. A similar algebraic sum of contributions due to different coordination geometries must occur also in CPL (see below). The relative magnitude of the various terms is not necessarily comparable for ECD and CPL, the former being dominated by exciton interactions, the latter by static and dynamic coupling of ligand/metal centred transitions. Moreover, different structures may not be equally emissive. These factors can explain why ECD/CPL signs are only partially correlated on comparing the spectra with different ligands.

On the contrary, although of somehow modest intensity, the ECD spectra of the complexes incorporating the three substituted coumarins are more defined, in particular for the CoumC-based

complex (Figures 7, 8, and 9, right). In all cases, the sequence of signs is the same: +-+ on going from lower to higher energies (for the R isomeric complex). This suggests that, at least for [Tb(bpcd)(CoumC)], there is a more definite stereochemical preference. Accordingly, from our DFT structural calculations (*vide supra*) the *trans*-O,O species of this complex is less stable than the other two possible *trans*-NN and *cis*-OO,NN isomers. On the contrary, in the case of [Tb(bpcd)(CoumA)] and [Tb(bpcd)(CoumB)] complexes, the three possible isomers are equally probable.

The mirror image relationship observed for all the UV-ECD spectra of enantiomer pairs witnesses the purity (chemical and stereochemical) of the compounds.

As for the CPL of the Tb(III) complexes, the spectra of the enantiomers are the mirror image of one another and the most prominent chiroptical signals are recorded for the $^5D_4 \rightarrow {}^7F_5$ manifold (around 546 nm), which gives rise, in all the cases, to an alternating sign three-line emission (figures 6-9, left).

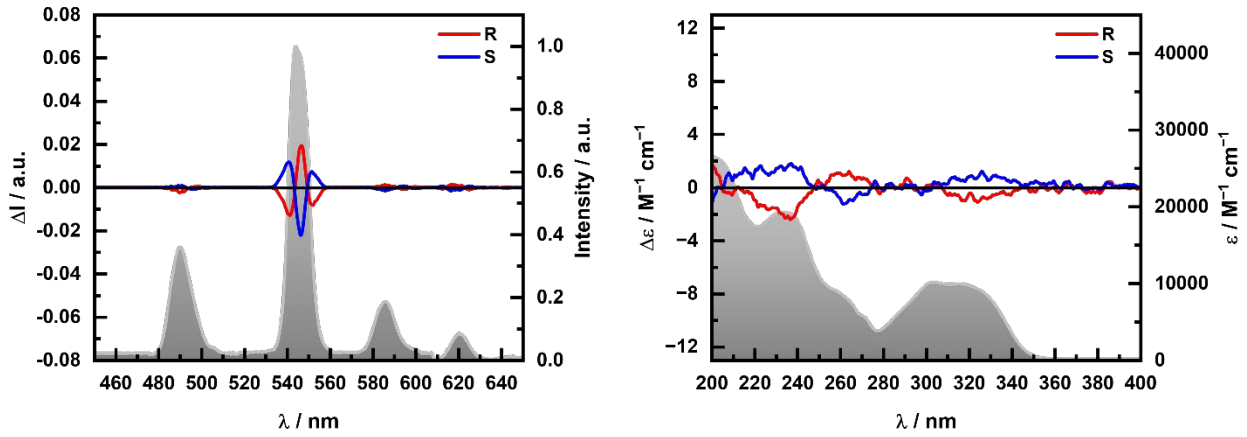

Figure 6. [Tb(bpcd)(Coum)]; **Left)** CPL spectra of both enantiomers between 450 and 650 nm, with the normalized total emission traced in the background (CPL and total emission are plotted in coherent units). **Right)** ECD spectra for both enantiomers (Δε) between 200 and 400 nm with the average total absorbance of the two enantiomers (ε) traced in the background.

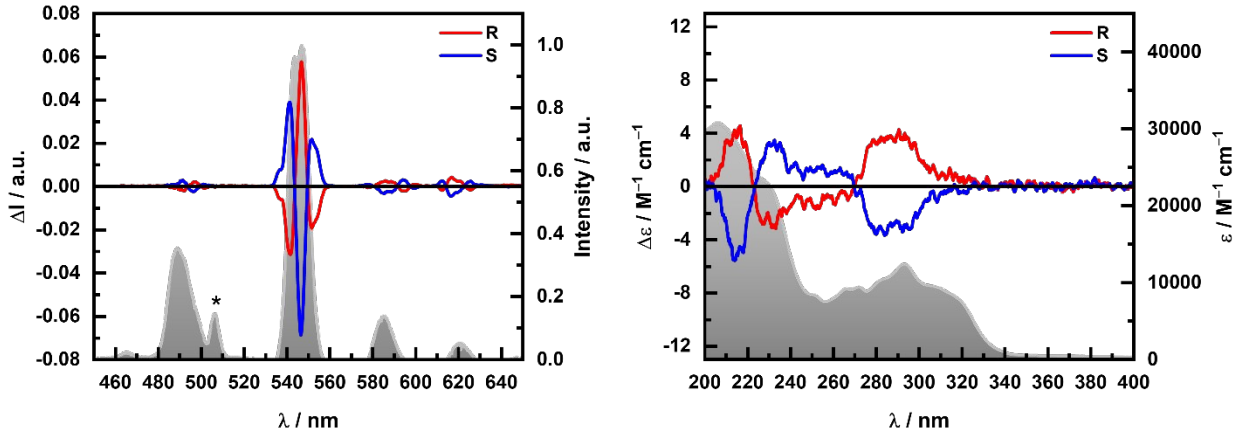

Figure 7. [Tb(bpcd)(CoumA)]; **Left)** CPL spectra of both enantiomers between 450 and 650 nm, with the normalized total emission traced in the background (CPL and total emission are plotted in coherent units). **Right)** ECD spectra for both enantiomers (Δε) between 200 and 400 nm with the average total absorbance of the two enantiomers (ε) traced in the background. The band at ca. 505 nm (left) marked with an asterisk is the harmonic of the excitation light.

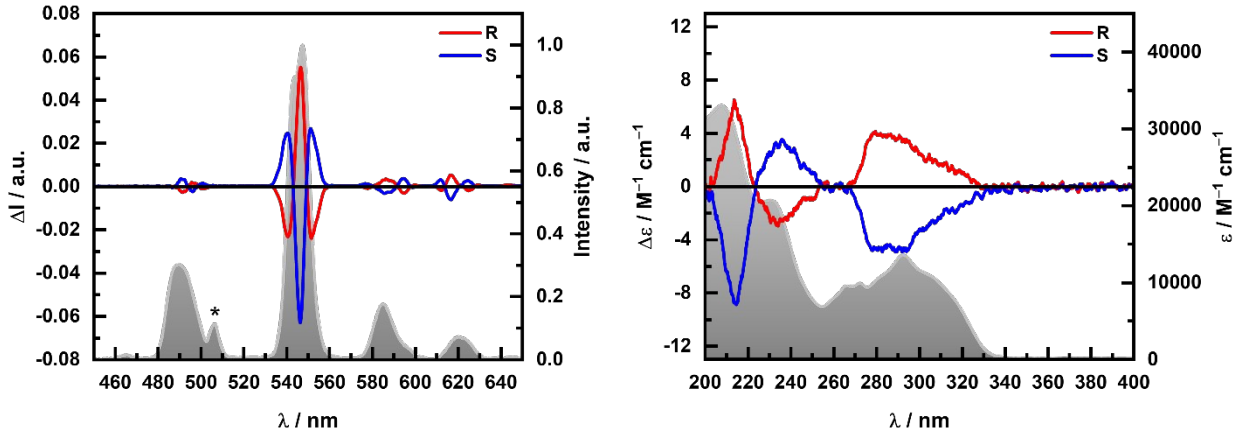

Figure 8. [Tb(bpcd)(CoumB)] **Left)** CPL spectra of both enantiomers between 450 and 650 nm, with the normalized total emission traced in the background (CPL and total emission are plotted in coherent units). **Right)** ECD spectra for both enantiomers (Δε) between 200 and 400 nm with the average total absorbance of the two enantiomers (ε) traced in the background. The band at ca. 505 nm (left) marked with an asterisk is the harmonic of the excitation light.

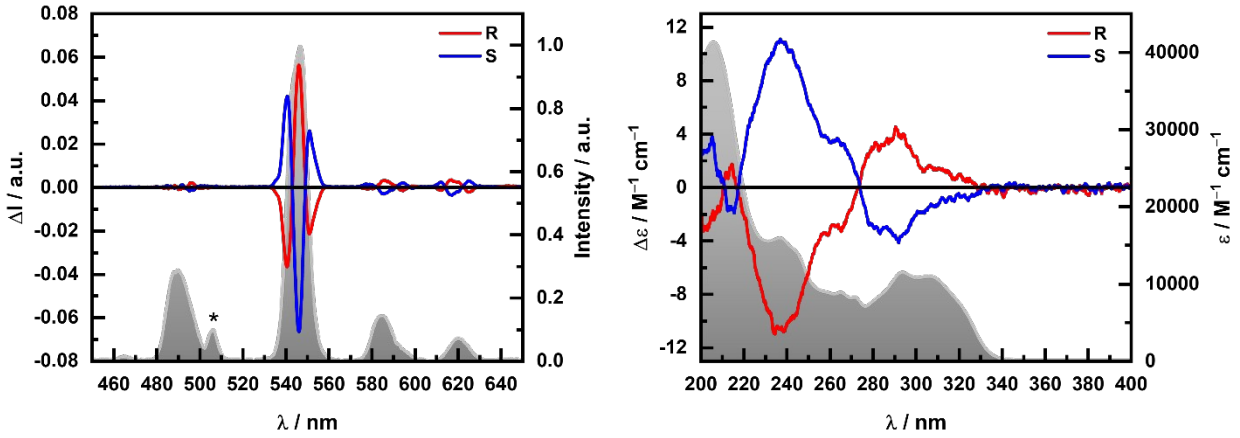

Figure 9. [Tb(bpcd)(CoumC)] **Left)** CPL spectra of both enantiomers between 450 and 650 nm, with the normalized total emission traced in the background (CPL and total emission are plotted in coherent units). **Right)** ECD spectra for both enantiomers (Δε) between 200 and 400 nm with the average total absorbance of the two enantiomers (ε) traced in the background. The band at ca. 505 nm (left) marked with an asterisk is the harmonic of the excitation light.

[Tb(bpcd)(CoumA)], [Tb(bpcd)(CoumB)] and [Tb(bpcd)(CoumC)] show g_{lum} factors (Table 4) at 547 nm three times higher than the one of [Tb(bpcd)(Coum)]. The g_{lum} values are around 0.06-0.07 for the former three complexes and 0.02 for Coum-based complex. This is in very good agreement with the above interpretation of the UV-ECD spectra, where we suggested that the derivatized coumarins provide more defined structures ([Tb(bpcd)(CoumC)], in particular), whereas [Tb(bpcd)(Coum)] is somewhat fluxional. Thus, not only the exciton coupling interactions is the average between oppositely signed contributions, but also the metal-centered CPL would be.

We must also notice that the CPL intensities and consequently the g_{lum} values reported here may be the result of cancellation between oppositely signed contributions of the $^5D_4 \rightarrow {}^7F_5$ manifold. Indeed, here we observed that it is composed of 3 apparent bands, which may partially cancel each other. Furthermore, we must consider that the total expected multiplicity of this manifold may reach 99 or, in the low temperature/high crystal field (CF) splitting regime at least 11 (originating from the lowest CF Stark level of $^5D_4$ and ending in each of the M_J components of $^7F_5$)

In conclusion, accepting the limits of experimental measurements, with the values of ε, □$_{ovl}$ and $|g_{lum}|$ reported in Table 3, we calculate B_{CPL} that reaches the maximum value for the [Tb(bpcd)(CoumB)] complex (45.5 at 547 nm; Table 4).[9,20]

Table 3. Photophysical (□ and □$_{ovl}$) and chiroptical (g_{lum} and B_{CPL}) parameters of CPL-active Tb(III) complexes investigated in this work.

Complex	$\varepsilon/M^{-1}cm^{-1}$ (λ_{abs}/nm)	ϕ_{ovl} (%)	Transition $^5D_4 \rightarrow {}^7F_J$	$\lvert g_{lum} \rvert$ (λ/nm)[b]	$B_{CPL}/M^{-1}cm^{-1}$[a]
[Tb(bpcd)](Coum)	12000 (313)	53	J = 6	0.004 (490)	/
				0.003 (498)	/
			J = 5	0.046 (537)	11.7
				0.021 (547)	12.0
				0.037 (555)	6.9
			J = 4	0.007 (586)	/
				0.013 (594)	/
				0.014 (600)	/
			J = 3	0.045 (613)	/
				0.023 (617)	/
				0.020 (625)	/
[Tb(bpcd)](CoumA)	12400 (293)	35	J = 6	0.006 (492)	/
				0.013 (497)	/
			J = 5	0.050 (541)	16.9
				0.066 (547)	27.4
				0.061 (552)	7.5
			J = 4	0.020 (585)	/
				0.030 (600)	/
			J = 3	0.078 (613)	/
				0.074 (618)	/
				0.061 (625)	/
[Tb(bpcd)](CoumB)	13500 (293)	65	J = 6	0.010 (492)	/
				0.010 (496)	/
				0.017 (501)	/
			J = 5	0.051 (540)	22.6
				0.060 (547)	45.5
				0.061 (551)	18.2
			J = 4	0.023 (578)	/
				0.019 (586)	/
				0.074 (595)	/

			J = 3	0.106 (616)	/
				0.043 (625)	/
[Tb(bpcd)](CoumC)	11500 (293)	26	J = 6	0.010 (496)	/
			J = 5	0.067 (541)	11.9
				0.062 (546)	17.5
				0.057 (551)	5.6
			J = 4	0.016 (579)	/
				0.021 (585)	/
				0.049 (594)	/
			J = 3	0.046 (618)	/
				0.059 (625)	/

[a] Calculated according to a modified formula (eq. S1),[25] see also SI for a detailed explanation.

[b] The plots of g_{lum} vs □ are reported in Figures S9-S12.

Conclusions

In this contribution, we demonstrated that the sensitization efficiency of the Tb(III) and Eu(III) luminescence is strongly dependent on the substitution in C(3) position of the hydroxycoumarin *antenna* ligand (namely Coum, CoumA, CoumB, and CoumC) in the heteroleptic Ln(III) complexes containing also the bpcd chiral ligand. This efficiency is higher for Tb(III) and reaches its maximum value in the case of [Tb(bpcd)](CoumB) (> 62% in methanol), than for Eu(III) where the η_{sens} is very low (lower than 10% for the complexes containing CoumA, B and C). Thanks to the theoretical study of the energy transfer dynamics, we found a possible explanation for this behavior. In particular, although CoumB and CoumA (chosen as representative ligands) exhibited a better resonant energy condition between their triplet level and the $^5D_4$ emitting level of Tb(III) if compared with the case of Eu(III) ion, CoumB (bearing a secondary amide substituent in C(3) position) is characterized by a smaller D(donor)-A(acceptor) distance (R_L). This can justify the lower sensitization efficiency of Tb(III) luminescence by CoumA (35%) if compared to CoumB (62%). In addition, it is interesting that the dominant energy transfer channel in the case of Tb(III) complexes involves the singlet excited state of the coumarin ligands (CoumB, in particular) (*i.e.* $[S_1 \rightarrow S_0] \rightarrow Tb(III)[^7F_6 \rightarrow ^5G_6]$) with a very high transfer rate (around 10^9 s^{-1}). On the contrary, the energy transfer *via* triplet state is dominant in the case of Eu(III) complexes with CoumA and B and in both cases involves the $^5D_1$ level of the lanthanide ion. Finally, as for the chiroptical properties of the complexes, the nature of the substituting groups seems to play an important role. In particular, a triple CPL activity for Tb(III) ion at 546 nm

is recorded when an ester or amide groups ($|g_{lum}|$ 0.06-0.07) replace an acetyl group ($|g_{lum}|$ 0.02) in

C(3) position. Similarly, a more pronounced ECD signal in the UV spectral region has been observed for CoumA, B, and C derivatives. All that suggests a more defined stereochemical preference among the possible isomeric species. This seems to be verified in the case of [Tb(bpcd)(CoumC)] complex for which our DFT structural study discloses that the *trans*-O,O species is less stable than the other two possible *trans*-NN and *cis*-OO,NN isomers.

In conclusion, our investigation shows how small changes in the molecular structure of an *antenna* ligand could have a dramatic effect on the optical and chiroptical properties of a lanthanide complex. This information is of crucial importance for the design of advanced chiroptical materials.

Acknowledgments

The authors thank the Italian Ministry of Education, University and Research for the funds (PRIN: Progetti di Ricerca di Rilevante Interesse Nazionale – Bando 2017 Prot. 20172M3K5N). O.G.W is grateful for the financial support received from the European Commission Research Executive Agency, Horizon 2020 Research and Innovation Programme under the Marie Sklodowska-Curie grant agreement No. 859752-HEL4CHIROLED-H2020-MSCA-ITN-2019.

Authors from the University of Parma benefited from the equipment and support of the COMP-HUB Initiative, funded by the "Departments of Excellence" program of the Italian Ministry for Education, University and Research (MIUR, 2018-2022). Authors from the University of Verona gratefully thank the Facility "Centro Piattaforme Tecnologiche" (CPT) to access the Fluorolog 3 (Horiba-Jobin Yvon) spectrofluorometer and Luca Zuppiroli, from the University of Bologna, department of Industrial Chemistry, for performing the mass spectrometry measurements. Moreover, they thank Capucine Nonis and Thomas Erbland, students from SIGMA Clermont - Université Clermont Auvergne, for participating at the development of the project during their internship in Verona. AM acknowledges the University of Udine for the grant "Ricerca Collaborativa" DM737/2001. AM and FP acknowledge the Italian Ministry of University and Research for the received funds [PRIN (Progetti di Ricerca di Rilevante Interesse Nazionale, Bando 2022 PNRR) project "TheCURA", Grant No. P20222TPZS]. This work was developed within the scope of the project CICECO- Aveiro Institute of Materials, UIDB/50011/2020, UIDP/50011/2020 & LA/P/0006/2020 and LogicALL (PTDC/CTMCTM/0340/2021) financed by Portuguese funds through the FCT/MEC (PIDDAC).

Supporting Information: Synthetic protocol and ^{1}H- and ^{13}C-NMR data of the coumarin ligands. ESI-MS data of the Tb(III), Eu(III) and Gd(III) complexes under investigation. Minimum energy structure of La(III)-based complexes. Energy level diagram of the investigated coumarin ligands, excitation and emission spectra of Tb(III) complexes. g_{lum}-vs-wavelength plots of the Tb(III) complexes under investigation. Chiroptical instrumentation and definition of the B_{CPL} formula employed in this work. Definition of the intramolecular energy transfer (IET) equations used in this work. Kohn−Sham molecular orbitals composition of S_1 and T_1 states for [La(bpcd)CoumA·H_2O] and [La(bpcd)CoumB·H_2O]. IET rates for [Ln(bpcd)CoumA·H_2O] and [Ln(bpcd)CoumB·H_2O] (Ln = Eu and Tb). Multiphonon rates between adjacent levels of Ln(III). Rate equations model and theoretical quantum yields calculations, including a Python code to perform the surfaces of quantum yield as a function of the intersystem crossing rate and lifetimes (τ_T and τ_S).

References

(1) Çoruh, N.; Riehl, J. P. Circularly Polarized Luminescence from Terbium(III) as a Probe of Metal Ion Binding in Calcium-Binding Proteins. *Biochemistry* **1992**, *31* (34), 7970–7976. https://doi.org/10.1021/bi00149a031.

(2) Abdollahi, S.; Harris, W. R.; Riehl, J. P. Application of Circularly Polarized Luminescence Spectroscopy to Tb(III) and Eu(III) Complexes of Transferrins. *J. Phys. Chem.* **1996**, *100* (5), 1950–1956. https://doi.org/10.1021/jp952044d.

(3) Yuasa, J.; Ohno, T.; Tsumatori, H.; Shiba, R.; Kamikubo, H.; Kataoka, M.; Hasegawa, Y.; Kawai, T. Fingerprint Signatures of Lanthanide Circularly Polarized Luminescence from Proteins Covalently Labeled with a β-Diketonate Europium(III) Chelate. *Chem. Commun.* **2013**, *49* (41), 4604–4606. https://doi.org/10.1039/c3cc40331a.

(4) Leonzio, M.; Melchior, A.; Faura, G.; Tolazzi, M.; Bettinelli, M.; Zinna, F.; Arrico, L.; Di Bari, L.; Piccinelli, F. A Chiral Lactate Reporter Based on Total and Circularly Polarized Tb(III) Luminescence. *New J. Chem.* **2018**, *42* (10), 7931–7939. https://doi.org/10.1039/c7nj04640e.

(5) Mizzoni, S.; Ruggieri, S.; Sickinger, A.; Riobé, F.; Guy, L.; Roux, M.; Micouin, G.; Banyasz, A.; Maury, O.; Baguenard, B.; Bensalah-Ledoux, A.; Guy, S.; Grichine, A.; Nguyen, X.-N.; Cimarelli, A.; Sanadar, M.; Melchior, A.; Piccinelli, F. Circularly Polarized Activity from Two Photon Excitable Europium and Samarium Chiral Bioprobes. *J. Mater. Chem. C* **2023**, *11* (12), 4188–4202. https://doi.org/10.1039/D2TC05362D.

(6) Frawley, A. T.; Pal, R.; Parker, D. Very Bright, Enantiopure Europium(III) Complexes Allow Time-Gated Chiral Contrast Imaging. *Chem. Commun.* **2016**, *52* (91), 13349–13352. https://doi.org/10.1039/c6cc07313a.

(7) Wong, H.-Y.; Lo, W.-S.; Yim, K.-H.; Law, G.-L. Chirality and Chiroptics of Lanthanide Molecular and Supramolecular Assemblies. *Chem* **2019**, *5* (12), 3058–3095. https://doi.org/10.1016/j.chempr.2019.08.006.

(8) Kitagawa, Y.; Wada, S.; Islam, M. D. J.; Saita, K.; Gon, M.; Fushimi, K.; Tanaka, K.; Maeda, S.; Hasegawa, Y. Chiral Lanthanide Lumino-Glass for a Circularly Polarized Light Security Device. *Commun Chem* **2020**, *3* (1), 1–5. https://doi.org/10.1038/s42004-020-00366-1.

(9) Willis, O. G.; Zinna, F.; Di Bari, L. NIR-Circularly Polarized Luminescence from Chiral Complexes of Lanthanides and d-Metals. *Angew. Chem. Int. Ed.* **2023**, *62* (25), e202302358. https://doi.org/10.1002/anie.202302358.

(10) Willis, O. G.; Petri, F.; Pescitelli, G.; Pucci, A.; Cavalli, E.; Mandoli, A.; Zinna, F.; Di Bari, L. Efficient 1400–1600 Nm Circularly Polarized Luminescence from a Tuned Chiral Erbium Complex. *Angew. Chem. Int. Ed.* **2022**, *61* (34), e202208326. https://doi.org/10.1002/anie.202208326.

(11) Mukthar, N. F. M.; Schley, N. D.; Ung, G. Strong Circularly Polarized Luminescence at 1550 Nm from Enantiopure Molecular Erbium Complexes. *J. Am. Chem. Soc.* **2022**, *144* (14), 6148–6153. https://doi.org/10.1021/jacs.2c01134.

(12) Willis, B.-A. N.; Schnable, D.; Schley, N. D.; Ung, G. Spinolate Lanthanide Complexes for High Circularly Polarized Luminescence Metrics in the Visible and Near-Infrared. *J. Am. Chem. Soc.* **2022**, *144* (49), 22421–22425. https://doi.org/10.1021/jacs.2c10364.

(13) Willis, O. G.; Pucci, A.; Cavalli, E.; Zinna, F.; Di Bari, L. Intense 1400–1600 Nm Circularly Polarised Luminescence from Homo- and Heteroleptic Chiral Erbium Complexes. *J. Mater. Chem. C* **2023**, *11* (16), 5290–5296. https://doi.org/10.1039/D3TC00034F.

(14) Dhbaibi, K.; Grasser, M.; Douib, H.; Dorcet, V.; Cador, O.; Vanthuyne, N.; Riobé, F.; Maury, O.; Guy, S.; Bensalah-Ledoux, A.; Baguenard, B.; Rikken, G. L. J. A.; Train, C.; Le Guennic, B.; Atzori, M.; Pointillart, F.; Crassous, J. Multifunctional Helicene-Based Ytterbium Coordination Polymer Displaying Circularly Polarized Luminescence, Slow Magnetic Relaxation and Room Temperature Magneto-Chiral Dichroism. *Angew. Chem. Int. Ed.* **2023**, *62* (5), e202215558. https://doi.org/10.1002/anie.202215558.

(15) Lefeuvre, B.; Mattei, C. A.; Gonzalez, J. F.; Gendron, F.; Dorcet, V.; Riobé, F.; Lalli, C.; Le Guennic, B.; Cador, O.; Maury, O.; Guy, S.; Bensalah-Ledoux, A.; Baguenard, B.; Pointillart, F. Solid-State Near-Infrared Circularly Polarized Luminescence from Chiral YbIII-Single-Molecule Magnet. *Chem. - A Eur. J.* **2021**, *27* (26), 7362–7366. https://doi.org/10.1002/chem.202100903.

(16) Adewuyi, J. A.; Schley, N. D.; Ung, G. Vanol-Supported Lanthanide Complexes for Strong Circularly Polarized Luminescence at 1550 Nm. *Chem. - A Eur. J.* **2023**, *29* (36), e202300800. https://doi.org/10.1002/chem.202300800.

(17) Geng, Y.; Trajkovska, A.; Culligan, S. W.; Ou, J. J.; Chen, H. M. P.; Katsis, D.; Chen, S. H. Origin of Strong Chiroptical Activities in Films of Nonafluorenes with a Varying Extent of Pendant Chirality. *J. Am. Chem. Soc.* **2003**, *125* (46), 14032–14038. https://doi.org/10.1021/ja037733e.

(18) Yang, Y.; Da Costa, R. C.; Smilgies, D. M.; Campbell, A. J.; Fuchter, M. J. Induction of Circularly Polarized Electroluminescence from an Achiral Light-Emitting Polymer via a Chiral Small-Molecule Dopant. *Adv. Mater.* **2013**, *25* (18), 2624–2628. https://doi.org/10.1002/adma.201204961.

(19) Zinna, F.; Pasini, M.; Galeotti, F.; Botta, C.; Di Bari, L.; Giovanella, U. Design of Lanthanide-Based OLEDs with Remarkable Circularly Polarized Electroluminescence. *Adv. Funct. Mater.* **2017**, *27* (1), 1603719–1603719. https://doi.org/10.1002/adfm.201603719.

(20) Arrico, L.; Di Bari, L.; Zinna, F. Quantifying the Overall Efficiency of Circularly Polarized Emitters. *Chem. - A Eur. J.* **2021**, *27* (9), 2920–2934. https://doi.org/10.1002/chem.202002791.

(21) Wong, K.-L.; Bünzli, J.-C. G.; Tanner, P. A. Quantum Yield and Brightness. *J. Lumin.* **2020**, *224*, 117256. https://doi.org/10.1016/j.jlumin.2020.117256.

(22) Zinna, F.; Di Bari, L. Lanthanide Circularly Polarized Luminescence: Bases and Applications. *Chirality* **2015**, *27* (1), 1–13. https://doi.org/10.1002/chir.22382.

(23) Piccinelli, F.; Nardon, C.; Bettinelli, M.; Melchior, A.; Tolazzi, M.; Zinna, F.; Di Bari, L. Lanthanide-Based Complexes Containing a Chiral Trans-1,2-Diaminocyclohexane (DACH) Backbone: Spectroscopic Properties and Potential Applications. *ChemPhotoChem* **2022**, *6* (2), e202100143. https://doi.org/10.1002/cptc.202100143.

(24) Weber, M. J. Radiative and Multiphonon Relaxation of Rare-Earth Ions in Y_2O_3. *Phys. Rev.* **1968**, *171* (2), 283–291. https://doi.org/10.1103/PhysRev.171.283.

(25) Ruggieri, S.; Mizzoni, S.; Nardon, C.; Cavalli, E.; Sissa, C.; Anselmi, M.; Cozzi, P. G.; Gualandi, A.; Sanadar, M.; Melchior, A.; Zinna, F.; Willis, O. G.; Di Bari, L.; Piccinelli, F. Circularly Polarized Luminescence from New Heteroleptic Eu(III) and Tb(III) Complexes. *Inorg. Chem.* **2023**, *62* (23), 8812–8822. https://doi.org/10.1021/acs.inorgchem.3c00196.

(26) Leonzio, M.; Melchior, A.; Faura, G.; Tolazzi, M.; Zinna, F.; Di Bari, L.; Piccinelli, F. Strongly Circularly Polarized Emission from Water-Soluble Eu(III)- and Tb(III)-Based Complexes: A Structural and Spectroscopic Study. *Inorg. Chem.* **2017**, *56* (8), 4413–4422. https://doi.org/10.1021/acs.inorgchem.7b00430.

(27) Zinna, F.; Bruhn, T.; Guido, C. A.; Ahrens, J.; Bröring, M.; Di Bari, L.; Pescitelli, G. Circularly Polarized Luminescence from Axially Chiral BODIPY DYEmers: An Experimental and Computational Study. *Chem. Eur. J.* **2016**, *22* (45), 16089–16098. https://doi.org/10.1002/chem.201602684.

(28) Frisch, M. J.; Trucks, G. W.; Schlegel, H. B.; Scuseria, G. E.; Robb, M. A.; Cheeseman, J. R.; Scalmani, G.; Barone, V.; Petersson, G. A.; Nakatsuji, H.; Li, X.; Caricato, M.; Marenich, A. V.; Bloino, J.; Janesko, B. G.; Gomperts, R.; Mennucci, B.; Hratchian, H. P.; Ortiz, J. V.; Izmaylov, A. F.; Sonnenberg, J. L.; Williams-Young, D.; Ding, F.; Lipparini, F.; Egidi, F.; Goings, J.; Peng, B.; Petrone, A.; Henderson, T.; Ranasinghe, D.; Zakrzewski, V. G.; Gao, J.; Rega, N.; Zheng, G.; Liang, W.; Hada, M.; Ehara, M.; Toyota, K.; Fukuda, R.; Hasegawa, J.; Ishida, M.; Nakajima, T.; Honda, Y.; Kitao, O.; Nakai, H.; Vreven, T.; Throssell, K.; Montgomery, J. A., Jr.; Peralta, J. E.; Ogliaro, F.; Bearpark, M. J.; Heyd, J. J.; Brothers, E. N.; Kudin, K. N.; Staroverov, V. N.; Keith, T. A.; Kobayashi, R.; Normand, J.; Raghavachari, K.; Rendell, A. P.; Burant, J. C.; Iyengar, S. S.; Tomasi, J.; Cossi, M.; Millam, J. M.; Klene, M.; Adamo, C.; Cammi, R.; Ochterski, J. W.; Martin, R. L.; Morokuma, K.; Farkas, O.; Foresman, J. B.; Fox, D. J. Gaussian 16, Rev. A.03. *Gaussian 16 Rev.A03 Wallingford, CT* **2016**.

(29) De Rosa, C.; Melchior, A.; Sanadar, M.; Tolazzi, M.; Duerkop, A.; Piccinelli, F. Isoquinoline-Based Eu(III) Luminescent Probes for Citrate Sensing in Complex Matrix. *Dalton Trans.* **2021**, *50* (13), 4700–4712. https://doi.org/10.1039/D1DT00511A.

(30) De Rosa, C.; Melchior, A.; Sanadar, M.; Tolazzi, M.; Giorgetti, A.; Ribeiro, R. P.; Nardon, C.; Piccinelli, F. Effect of the Heteroaromatic Antenna on the Binding of Chiral Eu(III) Complexes to Bovine Serum Albumin. *Inorg. Chem.* **2020**, *59* (17), 12564–12577. https://doi.org/10.1021/acs.inorgchem.0c01663.

(31) Wang, J.; Wang, Y.; Zhang, Zh. H.; Zhang, X. D.; Tong, J.; Liu, X. Zh.; Liu, X. Y.; Zhang, Y.; Pan, Zh. J. Syntheses, Characterization, and Structure Determination of Nine-Coordinate $Na[Y^{III}(Edta)(H_2O)_3]\cdot 5H_2O$ and Eight-Coordinate $Na[Y^{III}(Cydta)(H_2O)_2]\cdot 5H_2O$ Complexes. *J. Struct. Chem.* **2005**, *46* (5), 895–905. https://doi.org/10.1007/s10947-006-0216-9.

(32) Wang, J.; Hu, P.; Liu, B.; Xu, R.; Wang, X.; Wang, D.; Zhang, L. Q.; Zhang, X. D. Structural Determination of New Eight-Coordinate $NH_4[Eu^{III}(Cydta)(H_2O)_2]\cdot 4.5H_2O$ and $K_2[Eu_2^{III}(Pdta)_2(H_2O)_2]\cdot 6H_2O$ Complexes. *J. Struct. Chem.* **2011**, *52* (3), 568–574. https://doi.org/10.1134/S0022476611030188.

(33) Mondry, A.; Janicki, R. From Structural Properties of the Eu^{III} Complex with Ethylenediaminetetra(Methylenephosphonic Acid) (H_8EDTMP) towards Biomedical Applications. *Dalton Trans.* **2006**, No. 39, 4702–4710. https://doi.org/10.1039/B606420E.

(34) Lee, C. T.; Yang, W. T.; Parr, R. G. Development of the Colle-Salvetti Correlation-Energy Formula Into A Functional of the Electron-Density. *Phys.Rev.B* **1988**, *37* (2), 785–789. https://doi.org/10.1103/PhysRevB.37.785.

(35) Becke, A. D. A New Mixing of Hartree-Fock and Local Density-Functional Theories. *J.Chem.Phys.* **1993**, *98* (2), 1372–1377. https://doi.org/10.1063/1.464304.
(36) Andrae, D.; Häußermann, U.; Dolg, M.; Stoll, H.; Preuß, H. Energy-Adjusted Ab Initio Pseudopotentials for the Second and Third Row Transition Elements. *Theor. Chim. Acta* **1990**, *77* (2), 123–141. https://doi.org/10.1007/BF01114537.
(37) Cao, X.; Dolg, M. Segmented Contraction Scheme for Small-Core Lanthanide Pseudopotential Basis Sets. *J. Mol. Struct. - Theochem* **2002**, *581* (1), 139–147. https://doi.org/10.1016/S0166-1280(01)00751-5.
(38) Tomasi, J.; Mennucci, B.; Cammi, R. Quantum Mechanical Continuum Solvation Models. *Chem. Rev.* **2005**, *105* (8), 2999–3093. https://doi.org/10.1021/cr9904009.
(39) Carneiro Neto, A. N.; Moura, R. T. J.; Carlos, L. D.; Malta, O. L.; Sanadar, M.; Melchior, A.; Kraka, E.; Ruggieri, S.; Bettinelli, M.; Piccinelli, F. Dynamics of the Energy Transfer Process in Eu(III) Complexes Containing Polydentate Ligands Based on Pyridine, Quinoline, and Isoquinoline as Chromophoric Antennae. *Inorg. Chem.* **2022**, *61* (41), 16333–16346. https://doi.org/10.1021/acs.inorgchem.2c02330.
(40) Van Bay, M.; Hien, N. K.; Tran, P. T. D.; Tuyen, N. T. K.; Oanh, D. T. Y.; Nam, P. C.; Quang, D. T. TD-DFT Benchmark for UV-Vis Spectra of Coumarin Derivatives. *Vietnam J. Chem.* **2021**, *59* (2), 203–210. https://doi.org/10.1002/vjch.202000200.
(41) Carneiro Neto, A. N.; Teotonio, E. E. S.; de Sá, G. F.; Brito, H. F.; Legendziewicz, J.; Carlos, L. D.; Felinto, M. C. F. C.; Gawryszewska, P.; Moura, R. T.; Longo, R. L.; Faustino, W. M.; Malta, O. L. Chapter 310 - Modeling Intramolecular Energy Transfer in Lanthanide Chelates: A Critical Review and Recent Advances. In *Handbook on the Physics and Chemistry of Rare Earths*; Bünzli, J.-C. G., Pecharsky, V. K., Eds.; Elsevier, 2019; Vol. 56, pp 55–162. https://doi.org/10.1016/bs.hpcre.2019.08.001.
(42) Moura Jr., R. T.; Carneiro Neto, A. N.; Aguiar, E. C.; Santos-Jr., C. V.; de Lima, E. M.; Faustino, W. M.; Teotonio, E. E. S.; Brito, H. F.; Felinto, M. C. F. C.; Ferreira, R. A. S.; Carlos, L. D.; Longo, R. L.; Malta, O. L. JOYSpectra: A Web Platform for Luminescence of Lanthanides. *Optical Materials: X* **2021**, *11*, 100080. https://doi.org/10.1016/j.omx.2021.100080.
(43) Riseberg, L. A.; Moos, H. W. Multiphonon Orbit-Lattice Relaxation of Excited States of Rare-Earth Ions in Crystals. *Phys. Rev.* **1968**, *174* (2), 429–438. https://doi.org/10.1103/PhysRev.174.429.
(44) Miyakawa, T.; Dexter, D. L. Phonon Sidebands, Multiphonon Relaxation of Excited States, and Phonon-Assisted Energy Transfer between Ions in Solids. *Phys. Rev. B* **1970**, *1* (7), 2961–2969. https://doi.org/10.1103/PhysRevB.1.2961.
(45) Carneiro Neto, A. N.; Nasalska, J.; Gawryszewska, P.; Trush, V. A.; Sokolnicki, J.; Malta, O. L.; Legendziewicz, J. Intramolecular Energy Transfer and Its Influence on the Overall Quantum Yields of Eu3+ and Tb3+ Chelates with Dimethyl(Phenylsulfonyl)Amidophosphate Ligands. *Spectrochim. Acta A* **2025**, *324*, 124875. https://doi.org/10.1016/j.saa.2024.124875.
(46) Guzmán-Méndez, Ó.; González, F.; Bernès, S.; Flores-Álamo, M.; Ordóñez-Hernández, J.; García-Ortega, H.; Guerrero, J.; Qian, W.; Aliaga-Alcalde, N.; Gasque, L. Coumarin Derivative Directly Coordinated to Lanthanides Acts as an Excellent Antenna for UV–Vis and Near-IR Emission. *Inorg. Chem.* **2018**, *57* (3), 908–911. https://doi.org/10.1021/acs.inorgchem.7b02861.
(47) Yahiaoui, Z.; Hassairi, M. A.; Dammak, M.; Cavalli, E. Tunable Luminescence and near White-Light Emission of YPO4:Eu^{3+} ,Tb^{3+} ,Tm^{3+} Phosphors. *J. Alloys Compd.* **2018**, *763*, 56–61. https://doi.org/10.1016/j.jallcom.2018.05.317.
(48) Peacock, R. D. The Intensities of Lanthanide f ↔ f Transitions. In *Rare Earths SE - 3*; Springer Berlin Heidelberg, 1975; Vol. 22, pp 83–122. https://doi.org/10.1007/BFb0116556.
(49) Werts, M. H. V.; Jukes, R. T. F.; Verhoeven, J. W. The Emission Spectrum and the Radiative Lifetime of Eu^{3+} in Luminescent Lanthanide Complexes. *Phys. Chem. Chem. Phys.* **2002**, *4* (9), 1542–1548. https://doi.org/10.1039/B107770H.

(50) Thor, W.; Carneiro Neto, A. N.; Moura, R. T.; Wong, K.-L.; Tanner, P. A. Europium(III) Coordination Chemistry: Structure, Spectra and Hypersensitivity. *Coord. Chem.Rev.* **2024**, *517*, 215927. https://doi.org/10.1016/j.ccr.2024.215927.

(51) Holz, R. C.; De Horrocks, W. W.; Chang, C. A. Spectroscopic Characterization of the Europium(III) Complexes of a Series of N,N'-Bis(Carboxymethyl) Macrocyclic Ether Bis(Lactones). *Inorg. Chem.* **1991**, *30* (17), 3270–3275. https://doi.org/10.1021/ic00017a010.

(52) Tsaryuk, V. I.; Zhuravlev, K. P.; Gawryszewska, P. Processes of Luminescence Quenching in Europium Aromatic Carboxylates with the Participation of LMCT States: A Brief Review. *Coord. Chem. Rev.* **2023**, *489*, 215206. https://doi.org/10.1016/j.ccr.2023.215206.

(53) Moura, R. T.; Quintano, M.; Santos-Jr, C. V.; Albuquerque, V. A. C. A.; Aguiar, E. C.; Kraka, E.; Carneiro Neto, A. N. Featuring a New Computational Protocol for the Estimation of Intensity and Overall Quantum Yield in Lanthanide Chelates with Applications to Eu(III) Mercapto-Triazole Schiff Base Ligands. *Opt. Mater. : X* **2022**, *16*, 100216. https://doi.org/10.1016/j.omx.2022.100216.

(54) Moura Jr., R. T.; Oliveira, J. A.; Santos, I. A.; de Lima, E. M.; Carlos, L. D.; Aguiar, E. C.; Neto, A. N. C. Theoretical Evidence of the Singlet Predominance in the Intramolecular Energy Transfer in Ruhemann's Purple Tb(III) Complexes. *Adv. Theory Simul.* **2021**, *4* (3), 2000304. https://doi.org/10.1002/adts.202000304.

(55) Aquino, L. E. do N.; Barbosa, G. A.; Ramos, J. de L.; O. K. Giese, S.; Santana, F. S.; Hughes, D. L.; Nunes, G. G.; Fu, L.; Fang, M.; Poneti, G.; Carneiro Neto, A. N.; Moura, R. T. Jr.; Ferreira, R. A. S.; Carlos, L. D.; Macedo, A. G.; Soares, J. F. Seven-Coordinate Tb^{3+} Complexes with 90% Quantum Yields: High-Performance Examples of Combined Singlet- and Triplet-to-Tb^{3+} Energy-Transfer Pathways. *Inorg. Chem.* **2021**, *60* (2), 892–907. https://doi.org/10.1021/acs.inorgchem.0c03020.

(56) Manzur, J.; Fuentealba, P.; Gil, Y.; Pérez-Obando, J.; Morales Alfaro, J.; Vega Carvallo, A. I.; Aravena, D.; Santana, R. C. de; Carneiro Neto, A. N.; Spodine, E. Tuning the Emission of Homometallic Dy^{III}, Tb^{III}, and Eu^{III} 1-D Coordination Polymers with 2,6-Di(1H-1,2,4-Triazole-1-Yl-Methyl)-4-R-Phenoxo Ligands: Sensitization through the Singlet State. *Inorg. Chem.* **2023**, *62* (47), 19195–19207. https://doi.org/10.1021/acs.inorgchem.3c02201.

(57) Kasprzycka, E.; Trush, V. A.; Amirkhanov, V. M.; Jerzykiewicz, L.; Malta, O. L.; Legendziewicz, J.; Gawryszewska, P. Contribution of Energy Transfer from the Singlet State to the Sensitization of Eu^{3+} and Tb^{3+} Luminescence by Sulfonylamidophosphates. *Chem. - A Eur. J.* **2017**, *23* (6), 1318–1330. https://doi.org/10.1002/chem.201603767.

(58) Alaoui, I. M. Nonparticipation of the Ligand's First Triplet State in Intramolecular Energy Transfer in Eu^{3+} and Tb^{3+} Ruhemann's Purple Complexes. *J. Phys. Chem.* **1995**, *99* (35), 13280–13282. https://doi.org/10.1021/j100035a036.

(59) Hidalgo-Rosa, Y.; Santoyo-Flores, J.; Treto-Suárez, M. A.; Schott, E.; Páez-Hernández, D.; Zarate, X. Tuning the Sensitization Pathway $T_1 \rightarrow {}^5D_J$ in Eu-Based MOF through Modification of the Antenna Ligand. A Theoretical Approach via Multiconfigurational Quantum Calculations. *J. Lumin.* **2023**, *260*, 119896. https://doi.org/10.1016/j.jlumin.2023.119896.

(60) Santos, P. R. S.; Jesus, A. A. S. S.; Lima, W. B.; Arruda, J. G.; Faustino, W. M.; Felinto, M. C. F. C.; Sabino, J. R.; Brito, H. F.; Costa, I. F.; Moura Jr., R. T.; Carneiro Neto, A. N.; Malta, O. L.; Terraschke, H.; Teotonio, E. E. S. Shedding Light on Eu(III) β-Diketonate Compounds with 1,2-Bis(Diphenylphosphino)Ethane Oxide Ligand: An Optical Study. *Eur. J. Inorg. Chem.* **2024**, *27* (4), e202300660. https://doi.org/10.1002/ejic.202300660.

(61) Pham, Y. H.; Trush, V. A.; Carneiro Neto, A. N.; Korabik, M.; Sokolnicki, J.; Weselski, M.; Malta, O. L.; Amirkhanov, V. M.; Gawryszewska, P. Lanthanide Complexes with N-Phosphorylated Carboxamide as UV Converters with Excellent Emission Quantum Yield and Single-Ion Magnet Behavior. *J. Mater. Chem. C* **2020**, *8* (29), 9993–10009. https://doi.org/10.1039/D0TC01445A.

(62) Fonger, W. H.; Struck, C. W. Unified Model of Energy Transfer for Arbitrary Franck-Condon Offset and Temperature. *J. Lumin.* **1978**, *17* (3), 241–261. https://doi.org/10.1016/0022-2313(78)90059-5.

(63) Auzel, F.; De Sa', G. F.; de Azevedo, W. M. An Example of Concentration Sensitive Electron-Phonon Coupling in $\{(C_4H_4)_4N\}_3$ $Eu_xY_{1-x}(NCS)_6$ and a New Hypothesis for Self-Quenching. *J. Lumin.* **1980**, *21* (2), 187–192. https://doi.org/10.1016/0022-2313(80)90020-4.

(64) Yamada, N.; Shionoya, S.; Kushida, T. Phonon-Assisted Energy Transfer between Trivalent Rare Earth Ions. *J. Phys. Soc. Jpn.* **1972**, *32* (6), 1577–1586. https://doi.org/10.1143/JPSJ.32.1577.

Table of Contents (TOC)

Different substituents at C(3) position of the hydroxycoumarin ligand strongly affect optical and chiroptical properties of the related Tb(III) and Eu(III) complexes. The Tb(III) complex containing CoumB ligand [bearing a secondary amide substituent in C(3) position] exhibits the best features (62% of sensitization efficiency and $|g_{lum}|$ 0.06-0.07 at 546 nm, in methanol).